

# The impact of higher order modes on transverse mode instability in bent optical fiber amplifiers

Sajjad Vazeerpour<sup>1</sup>, Mahdi Shayganmanesh<sup>2\*</sup>, Davoud Dorrnian<sup>1</sup>

## Abstract

We present a new theoretical model for analyzing the impact of higher order modes on transverse mode instability in bent Yb-doped fiber amplifiers. The model indicates a comparative analysis of mode instability using the normalized propagation constant in both straight and bent fibers amplifiers. The impact of different bending radii, on bent fibers is investigated in the normalized propagation constant. The results are then compared with the straight fibers. Simulation analysis showed that the interference between the fundamental mode ( $LP_{01}$ ) and the first higher order mode ( $LP_{11}$ ) has the greatest effect on the mode instability, comparing the other modes. Considering all the existed modes, the behavior of mode instability in the fibers with different V-numbers are simulated and explained physically.

## Keywords

Fiber laser, Transverse mode instability, Bent fiber amplifier, Normalized propagation constant, Higher order modes

<sup>1</sup> Plasma Physics Research Center, Science and Research Branch, Islamic Azad University, Tehran, Iran.

<sup>2</sup> Department of Physics, Iran University of Science and Technology, Tehran, Iran.

\*Corresponding author: shaygan@iust.ac.ir

## 1. Introduction

The continuous wave fiber lasers and amplifiers are the most important high-power lasers. High power Yb-doped fiber laser has been used in many different applications as material processing, defense systems, scientific research, etc. due to the advantages including high efficiency, beam quality, and flexible operation [1, 2].

The fiber amplifiers have some limitations in achieving higher powers. These limitations are due to the transverse mode instability (TMI) effect and reduces the output beam quality. Based on some theoretical and experimental studies in this field, it is widely believed that instabilities are caused by the interaction between thermal effects and interference of spatial modes [3–5]. Andermahr et al. in 2010 for the first time explained the concept of “an optically induced long-period fiber grating”, and found that these gratings transfer the fundamental mode (FM) to higher order mode (HOM) [6]. Then, a numerical model was presented in which these interactions between the thermal effects and the interference of modes create gratings along the fiber. The induced grating can transfer energy between the modes and reduces the beam quality [7, 8]. The traveling refractive index grating is created by the optical field of two interfering modes with a slight frequency difference between them [8]. The experimental results of TMI indicates that just the fundamental mode ( $LP_{01}$ ) and the first higher order mode ( $LP_{11}$ ) are involved in large mode areas fibers, except for fibers with large V-numbers (V) [9], however; it hasn't been investigated theoretically yet. We cal-

culated the interference between the fundamental mode and the first higher-order mode in mode instability simulations, in recent report [10].

Using Kramers-Kronig and thermal effects, the beam propagation model has been presented for interacting modes [8]. Solving thermal equation and using thermo-optic effect, another model was offered in which the multi-mode behavior caused the limitation of maximum output power of fiber amplifier [9]. This limitation or TMI effect was observed in Large-Mode-Area active fibers in a high-power operation [11]. Nonlinear processes such as stimulated Brillouin scattering (SBS), stimulated Raman scattering (SRS), and stimulated thermal Rayleigh scattering (STRS) are also the problems in achieving a high power in Yb-doped fiber amplifiers [12–14]. Ward et al. presented a model based on STRS in 2012 [15]. In fiber input, FM has the largest share, but due to TMI along the fiber, it becomes HOM and, the output is largely in HOM. This TMI is caused by a STRS process. In 2013, Liang Dong presented a model using quasi-closed-form solution for TMI of STRS in optical fibers. This model was extremely successful in explaining TMI. Dong considered that the source of heat inside the straight fiber is due to the interfering modes through quantum defect heating, and with solving the heat equation, he obtained the nonlinear coupling coefficient [16]. Fibers with symmetric bend compensated claddings are a means to reducing TMI effect in high-power amplifiers and lasers. Using fibers with low numerical aperture (NA) or bending fiber with radius about 10 cm are also reported as techniques for controlling TMI [17–20]. There is another method

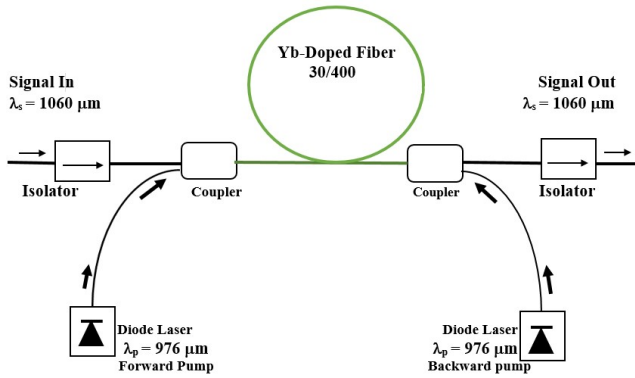


**Figure 1.** Schematic setup of a simple Yb-doped fiber amplifier.

to control TMI based on bi-directional pumping, which is presented by Chen Shi, Friedrich Moller etc. [21, 22]. Although this method optimally increases TMI threshold, due to the configuration of the opposite direction pumps in this arrangement, the possibility of optical damage to the pumping diodes increases. Rumao Tao et al. presented a semi-analytical model of STRS in which the behavior of TMI threshold power and the coupling maximum frequency was investigated as a function of the power [23].

In this work, we have been able to extend the previous models to obtain a new model simply analyzing TMI in higher order modes of bent fibers. Using the developed model here, we investigated the dependence of the bent radius on TMI parameters such as nonlinear coupling coefficient and TMI threshold power and compared the results to the straight fibers. Due to numerous applications of fiber bending, results of this work can be applicable in other fields in addition to fiber amplifiers as well.

## 2. Formulation and calculations

In this work, we use Yb-doped fiber amplifier as shown in Figure 1. The core and cladding radii ( $a, b$ ) of the fiber used are 15 and 200  $\mu\text{m}$ , respectively. We consider the fiber length to be one meter to simplify the calculations. The signal and pump wavelengths of the amplifier ( $\lambda_s, \lambda_p$ ) are 1060 and 976 nm, respectively. In Yb-doped fiber amplifiers, with increasing optical power, TMI occurs and the beam quality decreases. Due to the interference of modes inside the fiber, TMI begins.

According to Hansen [9], Dong [16] and many other papers, the interference pattern is formed along the fiber due to the interference of transverse modes. This pattern which acts as a longitudinal grating causes energy to be coupled from  $LP_{01}$  mode to the higher order mode ( $LP_{mn}$ ). The V-number of fiber used in this paper is 5.3348, in which  $LP_{01}, LP_{11}, LP_{21}, LP_{02}$  and  $LP_{31}$  are the modes propagated. Coupled nonlinear equation is obtained through solving the heat transportation equation for heat deposited by the interfering modes through quantum defect heat:

$$g_{01}\chi_{mn} = g_{01}(\chi_{mn}^r + i\chi_{mn}^i) = g_{01} \sum_{i=1}^{\infty} \frac{2(\frac{2\Omega}{\Gamma_{ml}} - i)}{1 + (\frac{2\Omega}{\Gamma_{ml}})^2} \chi_{mnl}$$

$$= \frac{2\pi k k_T}{\rho C} \left( \frac{\lambda_s}{\lambda_p} - 1 \right)$$

$$\sum_{i=1}^{\infty} \frac{2(\frac{2\Omega}{\Gamma_{ml}} - i) \int_0^d g f_{01}(r) f_{mn}(r) T_{ml}(r) r dr \int_0^b f_{01}(r) f_{mn}(r) T_{ml}(r) r dr}{1 + (\frac{2\Omega}{\Gamma_{ml}})^2 N_{01} N_{mn} \Gamma_{ml} \int_0^b T_{ml}^2(r) r dr} \quad (1)$$

According to Eq. (1), the main parameter of the coupled nonlinear equation is  $\chi_{mn}$ , which is called the nonlinear coupling coefficient.  $\chi_{mn}$  along the fiber is a fraction which converts  $g_{01}$  to  $g_{mn}$ . It depends on the quantum defect heat and the electric fields of modes, the physical parameters of the fiber. By reducing the quantum defect heat, the value of the nonlinear coupling coefficient decreases, and the modes field has got significant effect on  $\chi_{mn}$  value. The higher the value of the nonlinear coupling coefficient, the higher the probability of coupling the modes, therefore; TMI increases. Eq. (1) consists of three parts, the first part is the physical parameters of fiber and the second part indicates the quantum defect heat, and in the third part the temperature distribution due to the interference of transverse modes is described.

Where,  $f_{mn}(r)$  is the electric field in  $LP_{mn}$  mode,  $m$  and  $n$  represent azimuthal and radial modes order respectively and  $f_{01}(r)$  reveals the electric field in  $LP_{01}$  mode. The spatial temperature mode number of the heat transportation equation is  $l$ .  $T_{ml}(r)$  shows the spatial temperature mode, which is obtained from  $T_{ml}(r) \approx J_m[(\pi/4b)(4l - 1 + 2m)r]$ .  $J_m$  is Bessel function of the first kind. The parameter  $g = 9.7$  represents gain and  $g_{01} = 7.6$  stands for the gain coefficient corresponding to FM.  $N_{mn}$  and  $N_{01}$  are normalization factors in HOM and FM respectively, which is obtained from  $N_{mn} = \pi \int_0^{\infty} f_{mn}^2(r) r dr$ . The parameters  $k_0$  and  $2d$  are the wavenumber in the vacuum and doped-area diameters.  $\Omega/2\pi$  represents frequency separation between  $LP_{01}$  and  $LP_{mn}$  modes. Physical constants of fiber are Thermo-optics coefficient ( $K_T = 1.1 \times 10^{-5} \text{ K}^{-1}$ ), Density ( $\rho = 2.2 \times 10^3 \text{ kg/m}^3$ ), Specific heat ( $C = 741 \text{ J/kg/K}$ ) and Thermal conductivity ( $k = 1.38 \text{ w/m/K}$ ).  $\Gamma_{ml}$  denotes the heat damping factor, which is obtained from  $\Gamma_{ml} = (2k/\rho C)[q^2 + (\pi^2/16b^2)(4l - 1 + 2m)^2]$ .

Where  $\chi_{mnl}$  is the Nonlinear coupling coefficient amplitude and  $\chi_{mn}^r$  and  $\chi_{mn}^i$  are real, and imaginary of  $\chi_{mn}$ .

When the fiber is bent, the normalized propagation constant ( $b$ ) decreases comparing with the straight fiber and consequently the effective refractive index ( $n_{eff}$ ) and propagation constant decrease as well. The parameter  $b$ , in different transverse modes includes all the parameters related to the fiber geometry (Core diameter ( $2a$ ), Cladding diameter ( $2b$ ), bend radius and etc.) and material (core refractive index ( $n_{co}$ ),

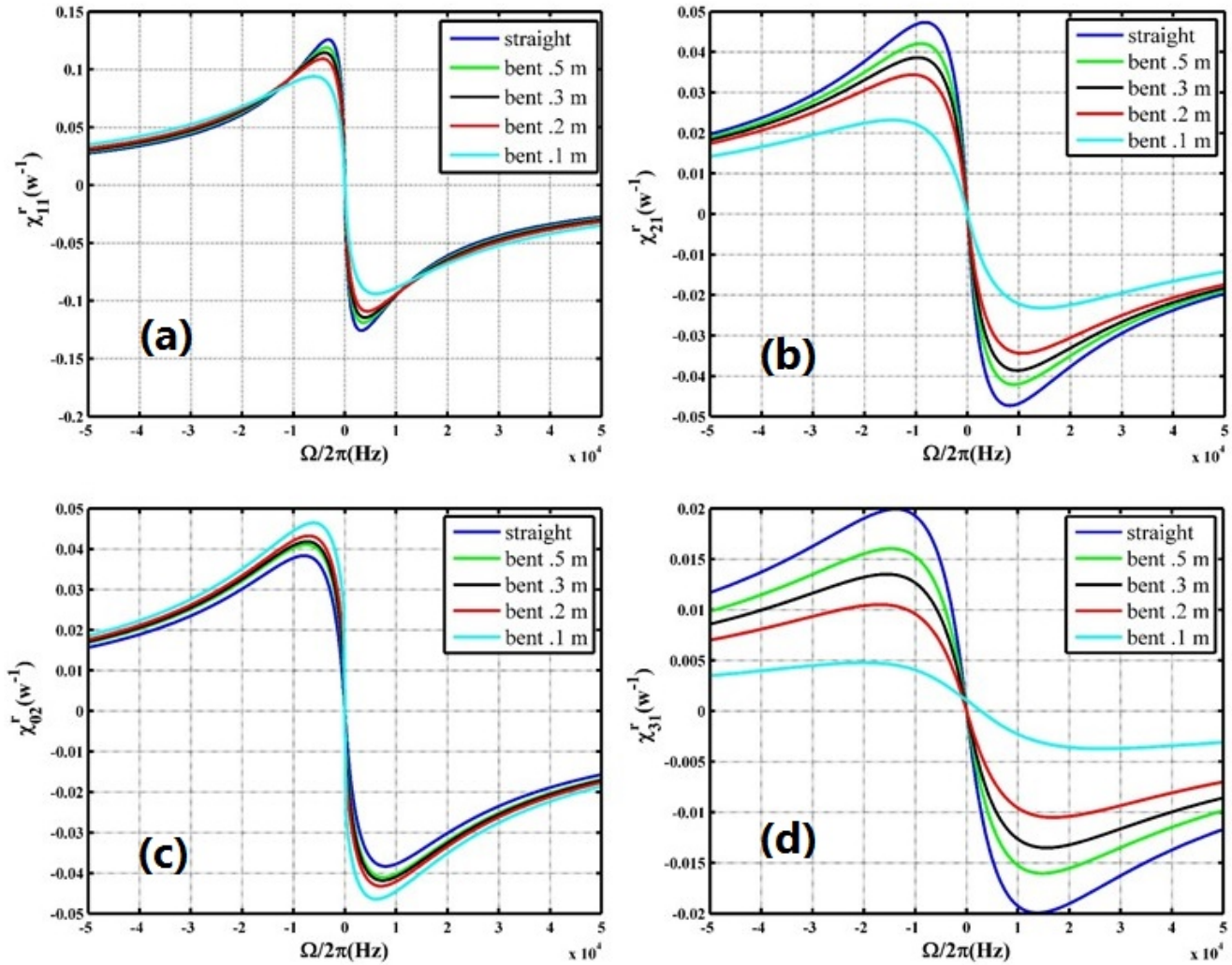


**Figure 2.** The real part of nonlinear coupling coefficient for  $LP_{mn}$  modes versus the frequency separation between modes of straight Yb-doped fibers in comparison with the bent Yb-doped fibers for  $R=0.1, 0.2, 0.3$  and  $0.5$  m. a)  $LP_{01}$ - $LP_{11}$ . b)  $LP_{01}$ - $LP_{21}$ . c)  $LP_{01}$ - $LP_{02}$ . d)  $LP_{01}$ - $LP_{31}$ .

cladding refractive index ( $n_{cl}$ ) and etc.). Therefore, in this paper, to investigate TMI in bent fibers, we used the normalized propagation constant as the base of calculations, which is completely different from the methods used in previous studies [24–27].

The normalized propagation constant is defined according to Equation  $b_{mn} = [n_{eff}^2 - n_{cl}^2] / [n_{co}^2 - n_{cl}^2]$  which varies between 0 and 1. If the effective refractive index tends toward  $n_{cl}$ ,  $b_{mn}$  value is 0, and if it tends toward  $n_{co}$ ,  $b_{mn}$  value is 1. The normalized propagation constant of bent glass fibers can be obtained by the following equation [24]:

$$b_{bmn} \cong b_{mn} - 1.575 \frac{a * n_{cl}^2}{R * NA^2} \tag{2}$$

Where,  $R$  is the bend radius,  $b_{mn}$  and  $b_{bmn}$  are the normalized propagation constant at the straight and bent fibers consequently. On the other hand, the relationship between the

normalized propagation constant of the straight fiber in the fundamental mode and the first-order mode, with the normalized frequency ( $V$ ) is obtained as follows [28]:

$$V = \frac{1}{\sqrt{1 - b_{mn}}} \left[ \frac{m\pi}{2} + \tan^{-1} \sqrt{\frac{b_{mn}}{1 - b_{mn}}} \right] \tag{3}$$

Where,  $b_{mn}$  is the normalized propagation constants in  $LP_{mn}$ . The numerical aperture ( $NA$ ) and the core refractive index are obtained:

$$NA = \frac{V}{ak_0} \tag{4}$$

$$n_{co} = \sqrt{n_{cl}^2 + NA^2} \tag{5}$$

The refractive index cladding ( $n_{cl}$ ) is taken as 1.4488. Therefore, according to Eq. (6), the effective refractive index in the

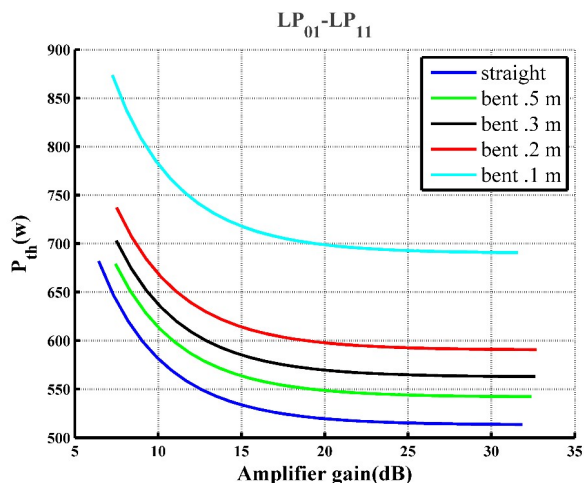


**Figure 3.** Comparing the threshold powers of straight and bent( $R=0.1, 0.2, 0.3$  and  $0.5$  m) Yb-doped fibers at  $x=1\%$ ,  $L=1$ m and  $P_{01}(0)/P_{11}(0) = 10^{30}$ .

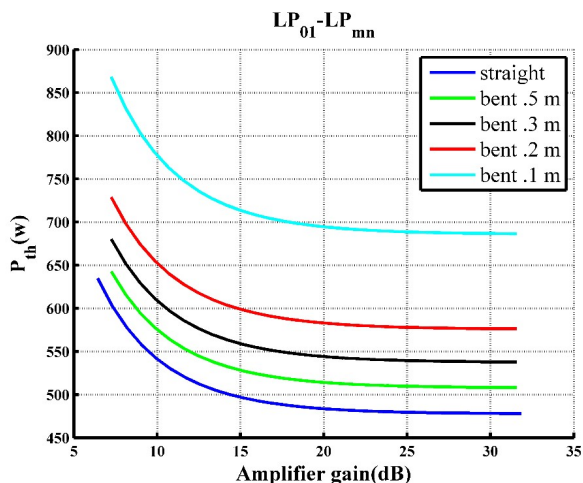


**Figure 4.** Comparing the threshold powers of straight and bent( $R=0.1, 0.2, 0.3$  and  $0.5$  m) Yb-doped fibers with calculating all higher-order modes at  $L=1$ m.

state of straight and bent is obtained:

$$n_{effmn} = [b_{mn}NA^2 + n_{cl}^2]^{\frac{1}{2}} \tag{6}$$

$$n_{effbm} = [b_{bm}NA^2 + n_{cl}^2]^{\frac{1}{2}}$$

Variations of the modes propagation constant due to bending affected the modes field distribution in both cladding and core of fiber. In the bent fibers, fluctuations in the modes field change the nonlinear coupling coefficient. The effective refractive index of each mode is obtained using the normalized propagation constant of the modes according to Eq. (6). The modes field for straight fiber can be found from Eq. (7):

$$f_{mn}(r) = \frac{J_m(ak_0^2(n_{co}^2 - n_{effmn}^2)r)}{J_m(a^2k_0^2(n_{co}^2 - n_{effmn}^2))}, a \geq r \geq 0$$

$$f_{mn}(r) = \frac{K_m(ak_0^2(n_{effmn}^2 - n_{cl}^2)r)}{K_m(a^2k_0^2(n_{effmn}^2 - n_{cl}^2))}, r > a \tag{7}$$

The modes field for bent fiber can be calculated by using bending parameters into Eq. (7) as well. Where,  $J_m$  represents Bessel functions of the first kind and  $K_m$  denotes the modified Bessel function of the second kind.

### 3. Straight and bend Yb-doped fiber amplifiers

#### 3.1 Transverse Mode instability (TMI)

In previous models developed by others, TMI in straight fibers have been studied [8, 9 and 16]. In order to investigate the modal instability in bent fibers, changes must be made in these models to be able to consider the effect of fiber bending. Usually, to achieve the appropriate beam quality in fiber lasers, low values are selected for the V-number, in which the number of transverse modes that can be propagated in the fiber will

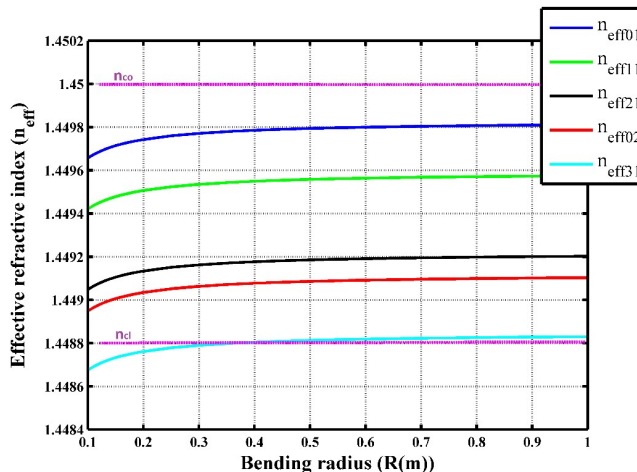


**Figure 5.** Influence of fiber bending radius on effective refractive index of transverse modes.

be low too. In literature, a combination of heat equation and wave propagation equation are used to investigate TMI in a manner that the thermal effects on the refractive index are considered in the wave propagation equation. The thermal effects are the result of quantum defect heat and the modes field intensity. The quantum defect heat depends on the wavelengths of the signal and the pump. Making physical changes to the fiber can change the mode field. Changing in the modes electric field causes a change in the modes propagation constant, followed by a change in the heat sources of the heat equation. We have generalized TMI to bent fibers by using the propagation constant of bent fiber in equations. Using the formulation of the section 2, TMI in higher order modes of the bent fibers can be analyzed. The propagation constant of the bent fiber should be calculated; then the nonlinear coupling coefficient of the bent fiber can be obtained.

First, the real part of nonlinear coupling coefficient ( $\chi'_{mn}$ )

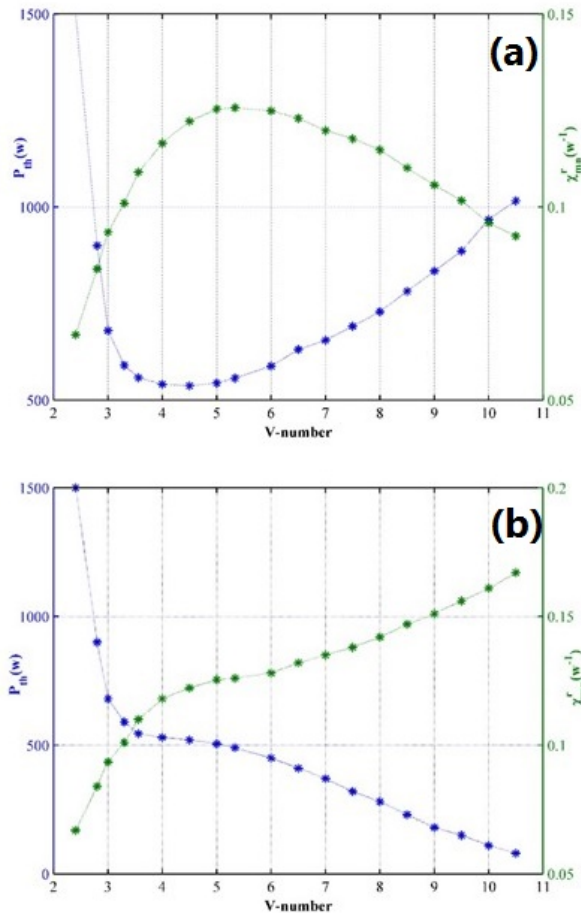


**Figure 6.** TMI threshold power and nonlinear coupling coefficient with respect to V-number under two conditions. a) Considering only two transverse modes LP<sub>01</sub> and LP<sub>11</sub>. b) Considering all transverse modes in calculations.

plotted according to the frequency separation ( $\Omega/2\pi$ ) between modes, then the peak of  $\chi'_{mn}$  is obtained in both straight and bent states used in calculations. In this model, Yb-doped fiber is bent at the radius of 0.1 m to 0.5 m and the results are compared with the straight fiber. In Figure 2(a), the real part of  $\chi_{11}$  is plotted according to the frequency separation between LP<sub>01</sub> and LP<sub>11</sub> modes in  $V = 5.3348$  and  $NA = 0.06$ .  $\Omega/2\pi$  at the peak of  $\chi'_{11}$  in Yb straight fiber is 3400 Hz. It decreases towards a higher frequency as a Lorentzian function. The real part of nonlinear coupling coefficient ( $\chi'_{11}$ ) demonstrates gain for LP<sub>11</sub> mode at the Stoke frequency. When bending radius are 0.1, 0.2, 0.3 and 0.5 m, the  $\Omega/2\pi$  values at the peak of  $\chi'_{11}$  = 6000, 4500, 4000 and 3750 Hz are obtained, respectively. As a result of bending the fiber, the frequency separation between LP<sub>01</sub> and LP<sub>11</sub> modes increases comparing to the straight fiber. while the bending radius increases, the frequency separation between modes decreases toward the amount of the straight fiber. Therefore; As the peak of  $\chi'_{mn}$  increases, the probability of mode coupling decreases and the

result is TMI decreasing as well.

Figure 2(b). shows  $\chi'_{21}$  versus  $\Omega/2\pi$  between LP<sub>01</sub> and LP<sub>21</sub> modes. The normalized propagation constant of LP<sub>21</sub> mode ( $b_{21}$ ) is about 0.372. The value of  $\chi'_{21}$  and  $\Omega/2\pi$  in straight fiber are obtained about 0.048 and 8200 Hz, respectively. When bending radius are 0.1, 0.2, 0.3 and 0.5 m, the values of the peak of  $\chi'_{21}$  = 14500, 10500, 9750 and 9000 Hz are obtained, respectively. According to Figure 2(c). with fiber bending, the behavior of LP<sub>02</sub> mode is different from other the higher order modes. As the bending radius decreases, the value of  $\chi'_{02}$  increases. When bending radius are 0.1, 0.2, 0.3 and 0.5 m, the values of the peak of  $\chi'_{02}$  = 6250, 7000, 7250 and 7900 Hz are obtained, respectively. The azimuthal mode number ( $m$ ) of LP<sub>01</sub> and LP<sub>02</sub> modes are the same and according to Eq. (7) have the same Bessel function. In Figure 2(d), the  $\chi'_{31}$  diagram versus  $\Omega/2\pi$  between LP<sub>01</sub> and LP<sub>31</sub> modes is plotted. Due to the low normalized propagation constant value of LP<sub>31</sub> mode in bent state, the value of  $\chi'_{31}$  with radius of 10 cm, tends to zero and can be ignored. When bending radius are 0.1, 0.2, 0.3 and 0.5 m, the values of the peak of  $\chi'_{31}$  = 20500, 17500, 16000 and 15000 Hz are obtained, respectively.

According to Eq. (8), the TMI threshold power decreases when  $P_{mn}(0)/P_{01}(0)$  and the gain increase. The TMI threshold power is plotted to gain in Figure 3.

$$P_L^{th} \approx \sum_{mn} \frac{1}{\chi_{mn}^r} \ln\left(\chi \frac{P_{01}(0)}{P_{mn}(0)}\right) \exp\left(\frac{1.25}{e^{801L}}\right) \quad (8)$$

Based on the above equation, the threshold is defined when the power in the LP<sub>mn</sub> mode reaches a certain fraction of the LP<sub>01</sub> mode at the output, i.e.,  $x = P_{mn}(L)/P_{01}(L)$ . As shown in Figure. 3, the power threshold of TMI is increased in the bent fiber and as the bending radius increases, the value of  $P_{01}^{th}$  declines and TMI occurs in the fiber amplifier earlier. For simplicity, we consider the fiber length equals to 1 m ( $L=1$ ). The power of each mode along the fiber ( $Z=0, Z=L$ ) is obtained double integrating the field intensity of the mode ( $\int \int I_{mn}(Z, r, \theta)$ ).

Figure 4, shows the power of the mode instability threshold considering all higher-order modes. TMI threshold begins at  $\sim 480$  w, in straight fibers and reaches  $\sim 700$  w due to bending the fiber with radius of 10 cm.

## 4. Results and Discussion

In this work we have presented a new model for analyzing TMI in all higher order modes of straight and bent optical fibers amplifiers. Our model has the advantage of Analysis simplicity and efficiency, and also TMI in Yb-doped amplifier has been investigated using the normalized propagation constant.

As aforementioned in first section, quantum defect heating is source of heat generation inside the fiber. This heat generates temperature gratings, and eventually leads to the traveling

temperature wave along the fiber. On the other hand, according to the thermo-optical properties, the refractive index is a function of temperature. Therefore, this generated temperature pattern forms the refractive index grating along the fiber. Temperature gratings increase the effective refractive index of the modes and thus, increase the normalized propagation constant of the modes. Using the equations and simulations presented in this model, the effective refractive index and the normalized propagation constant of higher order modes increases more than  $LP_{01}$  mode, and as a result, the difference of the normalized propagation constant between the modes decreases. The probability of coupling between the modes increases by reducing the normalized propagation constant difference between  $LP_{01}$  mode and the higher order modes. As the normalized propagation constant increases,  $LP_{mn}$  and  $LP_{01}$  modes are drawn to the core.

As can be concluded from Figure 2, by decreasing the bending radius of the fiber, the frequency separation ( $\Omega/2\pi$  at the peak of  $\chi'_{mn}$ ) between the fundamental and higher order modes increases and the nonlinear coupling coefficient decreases. However, the behavior of  $LP_{02}$  mode is different, and as the bending radius decreases, the separation frequency between  $LP_{01}$  and  $LP_{02}$  modes decreases and  $\chi'_{mn}$  increases. The separation frequency between the fundamental mode and the modes  $LP_{11}$ ,  $LP_{21}$ ,  $LP_{02}$  and  $LP_{31}$  in the straight fiber are 3400, 8200, 6500 and 14500 Hz, respectively. Through bending the fiber with radius of 10 cm, the separation frequency of the modes are obtained 6000, 14500, 6250, 20500 Hz, respectively. Considering the modes separation frequency values, the probability of  $LP_{11}$  mode coupling is the highest, and  $LP_{31}$  is the least.

As the frequency separation of modes increases, the coupling of modes decreases and as a result, according to Figures 3, 4, the threshold power of TMI increases. Figure 5, shows the changes of the effective refractive index of the modes with respect to the different radii of bending of the fiber at  $V = 5.3348$ . By reducing the bending radius of the fiber, the effective refractive index of the modes decreases and according to Eq. (6), the normalized propagation constant of the modes also decreases. Then, by reducing the effective refractive index, the modes are drawn towards the cladding and the higher order modes exits from the fiber. In bent fiber, the displacement of the intensity field of the higher order modes is higher than the fundamental mode in the direction of the horizontal diameter of the fiber core. Fiber bending works inversely to the heat behavior inside the fiber. The heat increases the normalized propagation constant of the modes and the modes move away from the cladding, but the bending of the fiber reduces the normalized propagation constant of the modes and the modes are drawn towards the cladding. Therefore, in any method proposed to control TMI, the normalized propagation constant of higher order modes should be reduced, or the difference between the normalized propagation constant of modes should be increased.

One of the issues related to calculation of TMI is the number

of assumed transverse modes in the model. For example Dong and Hansen, have stated in their articles that they have considered only two modes,  $LP_{01}$  and  $LP_{11}$ , in their calculations [9, 16]. In the following, we will examine this issue. First we assume that there are only two modes  $LP_{01}$  and  $LP_{11}$  in the fiber core, and therefore only the interference of these two modes is considered in calculations. In Figure 6(a), the power threshold of TMI and the nonlinear coupling coefficient are plotted in terms of the V-number. To analyze Figure 6a, the region of change of the V-number is divided into three parts. The first part is up to  $V = 3$ . As can be seen in the Figure 8a, the power instability threshold and the nonlinear coupling coefficient in the first part decrease and increase with a steep slope, respectively. The fiber with  $V = 2.4$  is a single-mode fiber, therefore this behavior is reasonable. In this way, with increasing V-number and thereafter increasing the core diameter, the probability of the presence of  $LP_{11}$  mode increases and therefore the power of the instability threshold decreases and the nonlinear coupling coefficient increases as well. In the second part, it is  $3 < V < 6$ . In this section, with increasing V-number, the radius of the fiber core continues to increase and therefore the possibility of the presence of modes higher than  $LP_{11}$  increases, but since the normalized propagation constant of the modes higher than  $LP_{11}$  is small, in practice the possibility of interference these modes with fundamental mode is low. Therefore, the assumption of calculations with only two modes is still valid, and as can be seen in the Figure 6(a), up to  $V = 6$  (exactly  $V = 5.8$ ) the behavior of the curves is still reasonable, and  $P_{th}$  and  $\chi'_{mn}$  are slightly decreasing and increasing, respectively. The third part of the graph is for  $V \geq 6$  region. As can be seen in the Figure 6(a), if we continue to consider only two modes for calculating TMI, we will reach an unreasonable result. As shown in Figure 6(a), in the region  $V > 6$ ,  $P_{th}$  increases and  $\chi'_{mn}$  decreases, which physically can not be correct. The reason is that in this region, with further increase of the radius of the fiber core, modes higher than  $LP_{11}$  are present and have a large normalized propagation constant that needs to be considered in the calculations, but in the calculations only  $LP_{01}$  and  $LP_{11}$  are considered.

For better investigation, a more accurate simulation is also conducted. Modal instability power threshold and nonlinear coupling coefficient with respect to different V-numbers is presented in Figure 6(b). This time we have considered all the transverse modes in the fiber in different V-numbers in the calculations. For the sake of simplicity, the interference of different polarizations and the interference of higher order modes with each other are eliminated. The diagram obtained in Figure 6(b) is different from Figure 6(a). Although the first part of Figure. 6b is similar to Figure. 6a, since there is no higher order modes except  $LP_{11}$ . In the second part the threshold power decreases with a gentle slope. This is because the normalized propagation constant of the higher modes in the second part is small compared to the fundamental mode. Dong and Hansen's approximation [9, 16] in considering two modes in calculations at  $V < 6$  is almost correct, and higher-

order modes have little contribution to TMI. In the previous sections of this paper also we have used this approximation to simplify the equations. In this paper, we have obtained the threshold power considering the mentioned approximation for straight fiber  $\sim 520$  w, but without the approximation, threshold power is  $\sim 490$  w. The third part of Figure 6(b) is completely different from Figure 6(a). The threshold power of TMI is decreasing with a steep slope and the nonlinear coupling coefficient is increasing. In this region, the normalized propagation constant of higher order modes increases and it is necessary to consider presence of higher order modes and the possibility of their interference with the fundamental mode. As can be seen, the third region of Figure 6(b), unlike Figure 6(a), is quite reasonable.

## 5. Conclusion

In this paper, we presented a new model for investigating TMI in bent fibers. The results revealed that by decreasing the bending radius, the normalized propagation constant of the mode diminished causing reduced propagation constant and effective refractive index of the fiber whereby the laser modes tended to the cladding fiber. As the bending radius shrank, the frequency separation between two modes increased, resulting in lowered coupling nonlinear coefficient and enhanced threshold power of TMI.

**Disclosures:** This research did not receive any specific grant from funding agencies in the public, commercial, or not-for-profit sectors.

### Conflict of interest statement:

The authors declare that they have no conflict of interest.

## References

- [1] M.N. Zervas. *Int. J. Mod. Phys. B.*, **32**:1442009, 2014.
- [2] W. Shi, A. Schulzgen, R. Amezcua, X. Zhu, and S. U. Alam. *J Opt Soc Am B.*, **34**:FLA1, 2017.
- [3] M.N. Zervas. *APL Photonics*, **4**:022802, 2019.
- [4] A.V. Smith and J.J. Smith. *Opt. Express*, **21**:15168, 2013.
- [5] C. Jauregui, C. Stihler, and J. Limpert. *Adv. Opt. Photonics*, **12**:429, 2020.
- [6] N. Andermahr and C. Fallnich. *Opt. Express*, **18**:4411, 2010.
- [7] C. Jauregui, T. Eidam, J. Limpert, and A. Tunnermann. *Opt. Express*, **19**:3258, 2011.
- [8] A.V. Smith and J.J. Smith. *Opt. Express*, **19**:10180, 2011.
- [9] K.R. Hansen, T.T. Alkeskjold, J. Broeng, and J. Laegsgaard. *Opt. Express*, **21**:1944, 2013.
- [10] S.Vazeerpour, M.Shayganmanesh, and D.Dorranian. *Opt. Pura Apl.*, **54**, 2021.
- [11] B. Ward, C. Robin, and I. Dajani. *Opt. Express*, **20**:11407, 2012.
- [12] S.P. Singh, R. Gangwar, and N. Singh. *Prog. Electromagn. Res.*, **74**:379, 2007.
- [13] D. Chowdhury 2: 1 2010 A. Kobyakov, M. Sauer. *Adv. Opt. Photonics*, **2**:1, 2010.
- [14] T. Zhu, X. Bao, L. Chen, H. Liang, and Y. Dong. *Opt. Express*, **18**:22958, 2010.
- [15] B.G. Ward. *Opt. Express*, **21**:12053, 2013.
- [16] 2013. L. Dong, 21: 2642. *Opt. Express*, **21**:2642, 2013.
- [17] J.M. Fini and J.W. Nicholson. *Opt. Express*, **21**:19173, 2013.
- [18] C. Xie, T. Ning, L. Pei, S. Ma, J. Zheng, J. Xu, and S. Hou. *Opt. Fiber Technol.*, **52**:101953, 2019.
- [19] F. Zhang, H. Xu, Y. Xing, S. Hou, Y. Chen, J. Li, N. Dai, H. Li, Y. Wang, and L. Liao. *Laser Phys. Lett.*, **16**:035104, 2019.
- [20] K. Hejaz, A. Norouzey, R. Poozesh, A. Heidariazar, A. Roohforouz, R. Rezaei Nasirabad, N. Tabatabaei Jafari, A. Hamedani Golshan, A. Babazadeh, and M. Lafouti. *Laser Phys.*, **24**:025102, 2014.
- [21] C. Shi, R. Tao Su, H.W. Zhang, B.L. Yang, X.L. Wang, P. Zhou, X. Jun, and Q. Sheng Lu. *IEEE Photonics J.*, **9**:1502910, 2017.
- [22] F. Moller, R.G. Kramer, C. Matzdorf, S. Nolte, M. Strecker, F. Stutzki, M. Plötner, V. Bock, T. Schreiber, and A. Tünnermann. *ASSL. USA, AM2A*, **3**, 2018.
- [23] R. Tao, X. Wang, P. Zhou, and Z. Liu. *J. Opt.*, **19**:065202, 2017.
- [24] R.T. Schermer. *Opt. Express*, **15**:15674, 2007.
- [25] M.N. Zervas. *SPIE LASE. USA*, :1051205, 2018.
- [26] F. Beier, C. Hupel, S. Kuhn, S. Hein, J. Nold, F. Proske, B. Sattler, A. Liem, C. Jauregui, J. Limpert, N. Haarlammert, T. Schreiber, R. Eberhardt, and A. Tünnermann. *Optics Express*, **25**:14892, 2017.
- [27] Q. Chu, R. Tao, H. Lin, J. Wang, and F. Jing. *Sixth Symposium on Novel Optoelectronic Detection Technology and Applications*, :1145545, 2020.
- [28] K. Okamoto. *Fundamentals of Optical Waveguides*. Elsevier Inc, 2th edition, 2005.